INFLUENCE OF THE FINAL THERMAL SEALING ON THE PROPERTIES OF COMBINED ANODIC ALUMINA/CERIUM CONVERSION COATINGS ON AA2024-T3 AIRCRAFT ALLOY

Christian Girginov[1], Stephan Kozhukharov[1], Alexandar Tsanev[2], Michaela Georgieva[3,4], Maria Petrova[4], Emil Lilov[1], Plamen Petkov[1]

[1]*Faculty of Chemical Technologies*
University of Chemical Technology and Metallurgy
8 Kliment Ohridski blvd., 1756 Sofia, Bulgaria
[2]*Institute of General and Inorganic Chemistry*
Bulgarian Academy of Sciences, Acad. G. Bonchev Str. bl. 11
1113 Sofia, Bulgaria
[3]*Department of Chemistry*
Faculty of Electronic Engineering and Technologies
Technical University of Sofia, 8 Kliment Ohridski blvd.
1756 Sofia, Bulgaria
[4]*Department of Electrochemistry and Corrosion*
Institute of Physical Chemistry, Bulgarian Academy of Sciences
"Acad. G. Bonchev" Str., Block 11, 1113 Sofia, Bulgaria
E-mail: girginov@uctm.edu

Received 07 March 2023
Accepted 30 April 2023

ABSTRACT

The current research presents results following corrosion tests, performed on combined anodic alumina/cerium conversion coatings (Al_2O_3/CeCC), thermally sealed for 15 min at 100°C either in boiling water or in hot-air medium. The coatings were formed on AA2024-T3 aircraft alloy substrates, at the optimum conditions of anodization and cerium conversion coating deposition, described in previous works. Prior to the corrosion tests, both the color characteristics and wetting ability of the combined films were evaluated. The corrosion protective properties of the sealed films were assessed by means of Electrochemical Impedance Spectroscopy (EIS) and Potentiodynamic Polarization (PDP). The measurements were performed after 672 hours of exposure to a 5 % NaCl model corrosive medium (MCM). Additional long term (up to 1344 hours of exposure) durability tests were then performed under the same conditions for the samples and superior performance was established. The electrochemical measurements were conducted regularly, once a week. Low- and high-resolution Scanning Electron Microscopy (SEM) studies were performed on selected samples. The experimental results have shown that the sealing procedure in an aqueous environment enhances the corrosion protective ability and durability of the coating, probably due to formation of a hydrate layers, that suppresses the access of corrosive species to the surface of the substrate. This inference was additionally confirmed by the subsequent chemical analysis by means of X-Ray Photoelectron Spectroscopy (XPS). The results acquired have also shown that the incorporated Ce is predominantly in the form of Ce(IV)-oxides/hydroxides and after the thermal treatment almost entirely consists of cerium.

Keywords: AA2024T3 aircraft alloy, anodization, cerium conversion coatings, thermal sealing, corrosion resistance.

INTRODUCTION

There is strong evidence in recent years that lanthanides can be successfully used as cathodic corrosion inhibitors for the protection of highly-doped aluminum alloys and also that cerium compounds are the most effective among them [1]. Besides, these compounds can be successfully used as coating primer components [2 - 6]. The superior efficiency in inhibiting corrosion, as mentioned in these statements, has sparked extensive research into the application of various cerium compounds as corrosion inhibitors [7 - 22] and coating components [23 - 30].

On the other hand, anodization is an established

and efficient method used for the electrochemical formation of oxide layers on aluminum [31 - 33], copper [34], zinc [35, 36], titanium, [37, 38] and other valve metals [39, 40]. Indeed, it was recently shown that the combination of formation of cerium conversion coatings with anodization enables the successful formation of combined Al_2O_3/CeCC coating primers [41]. The final sealing of the already formed anodized films, also contributes to the extension of the durability of the coating primer [42, 43].

The aim of the present research is to analyze the effect of the final thermal treatment of these combined layers on their corrosion protective ability after 672 hours of exposure to a 5 % NaCl model corrosive medium (MCM). Further, the samples showing superior performance in the MCM were submitted to long-term tests (up to 1344 hours) in order to evaluate their durability. Both these characteristics (corrosion protective ability and durability) were evaluated by two analytical electrochemical techniques, namely Electrochemical Impedance Spectroscopy (EIS) and Potentiodynamic Polarization (PDP).

Further analyses were performed in order to evaluate the film's properties (color and wettability) and topology, by SEM and XPS methods.

EXPERIMENTAL

Sample preparation and treatment

Twelve samples cut from the AA2024-T3 aircraft alloy were subjected to three subsequent coating procedures in order to acquire identical Al_2O_3/CeCC double-layer coatings with similar features to those described in an earlier work [41]. The coating procedures and the respective conditions are shown in Table 1.

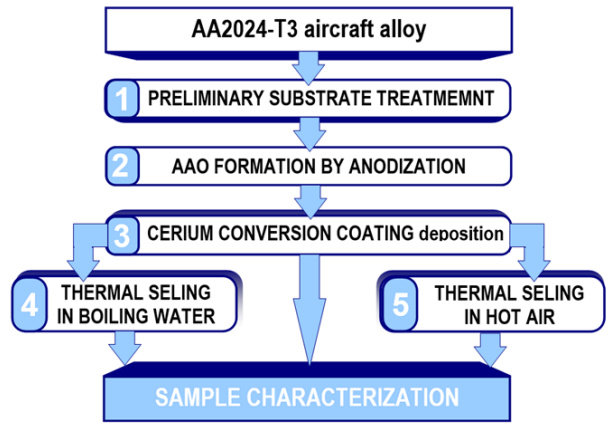

Fig. 1. Illustration of the sample treatment procedures sequence.

After carrying out all of the above-described treatments, the coated AA2024-T3 specimens were divided into three groups of four samples each, in order to be subjected to different final sealing procedures. Hence, the specimens have undergone different final sealings, forming three groups, enabling systematic comparative research activities. The sequence of the sample treatment steps is illustrated in Fig 1.

The sealing conditions and the sample group codes are shown in Table 2.

Coating characterization techniques

Color characteristics

The color parameters of all samples were recorded using a *Lovibond* tintometer (UK). Two measurements were performed at different sites on the surface of each sample. The purpose was to determine the repeatability between each two results, acquired from one and the same sample, in order to detect any variation. The

Table 1. Procedure for initial sample preparation.

Type of treatment	Solution composition	Duration	Temperature	Additional note
Preliminary treatment	50 g dm^{-3} NaOH	2 min	50°C	
	HNO_3:H_2O, $1:1_{v/v}$	2 min	Room	
	Double-distilled water	1 min	Room	
Anodization	15 wt.% H_2SO_4	50 min	20°C	15 mA cm^{-2}
Ce-conversion coating deposition	0.025 M $CeCl_3$ 0.025 M $(NH_4)_2Ce(NO_3)_5$ 10 cm^3 dm^{-3} 30 % H_2O_2	5 min	50°C	

Table 2. Conditions for sealing of the coatings.

Sample group	Coating sealing
G1-R*ef*	No sealing
G_2-BW	15 min in boiling distilled water
G_3-HA	15 min in ambient air at 100 ± 2°C

data were acquired in the widely used CIE L*, a*, b* three-coordinate color system [41, 44] and were further statistically evaluated.

Contact angle measurements

The respective contact angle measurements were performed using a *Theta Lite* high precision optical device, produced by Biolin Scientific (UK), coupled with specialized "One attention" software (Finland). The constant volume of the drops was ensured using a "Gastight 1001" precise screw syringe, product of Hamilton Co. (USA).

Comparative assessment of the corrosion protective properties

Electrochemical assessments of the films were performed on three samples of each group. The measurements were carried out after 672 hours of exposure to a 5 % NaCl solution, in three-electrode electrochemical cells, with a volume of 100 ml. The conventional electrochemical analytical techniques used were *Electrochemical Impedance Spectroscopy* (EIS) and *Potentiodynamic polarization* (PDP).

The EIS spectra acquisitions were performed on an Autolab 30 PG-stat, equipped with a Frequency Response Analyzer FRA-2 module. All measurements were performed against an Ag/AgCl/3M KCl reference electrode, positioned 10 mm above the corrosion test areas (CTA, 1 cm^2) of the specimens. The input excitation signals were introduced to the electrochemical cells by a cylindrical platinum mesh mounted around the reference electrode.

The PDP curves were acquired in the potential range from -50 to +500 mV versus a reference electrode, with a potential sweep of 10 mV s^{-1}. The samples found to have superior performance were subjected to extensive durability testing. This testing consisted of exposure to the above mentioned 5 % NaCl model corrosive medium for durations of up to 1344 hours, combined with regular (once a week) electrochemical assessments by means of EIS and PDP.

Topological observations

The surfaces of the specimens were observed using a scanning electron microscope (SEM), model JEOL JSM 6390. The images were acquired under conditions of secondary electron (SE) image acquisition, where the applied voltage was 120 kV, I ~ 100 μA.

Compositional analysis

The composition and electronic structure of the films were investigated by means of X-ray photoelectron spectroscopy (XPS). The measurements were carried out on an AXIS Supra electron-spectrometer (Kratos Analytical Ltd.), using achromatic AlKα radiation with a photon energy of 1486.6 eV. The energy calibration was performed by normalizing the C1s adsorption line of hydrocarbons to 284.6 eV. The binding energies (BE) were determined with an accuracy of ±0.1 eV. The changes in the composition of the films in depth were determined by monitoring areas of local photoelectron peaks at the binding energies of C1s, O1s, Ce3d, Al2p. Using the commercial data-processing software of Kratos Analytical Ltd., the concentrations of the different chemical elements (in at. %) were calculated by normalizing the areas of the photoelectron peaks to their relative sensitivity factors.

RESULTS AND DISCUSSION

Initial surface characterizations

Prior to investigating the chemical composition of the sealed Al_2O_3/CeCC coatings and their performance in the model corrosive medium, the samples were submitted to initial characterizations. These included colorimetric measurements and wetting tests. The acquired data underwent statistical treatment in order to obtain the respective confidential ranges of the measured values. The statistical data treatment approach is well-described and illustrated in previous works [41, 44, 45]. In order to collect sufficient data, each measurement was performed twice, so that eight results were acquired for each set of samples. Further, the results were statistically treated, assuming a *Student's* criterion of t = 5.041, corresponding to 8 measurements with a probability of P = 0.1 %. The final statistical results are summarized in Table 3.

Table 3. Final statistically acquired results by the colorimetric and wettability assessments.

Sample group	L^*_{av}	a^*_{av}	b^*_{av}	θ_{av}
G_1-Ref	82.86 ± 0.04	-3.910 ± 0.020	44.21 ± 0.01	39.40 ± 0.04
G_2-BW	84.15 ± 0.01	-5.361 ± 0.040	30.99 ± 0.04	14.52 ± 0.01
G_3-HA	86.30 ± 0.20	-5.031 ± 0.009	28.96 ± 0.01	35.97 ± 0.03

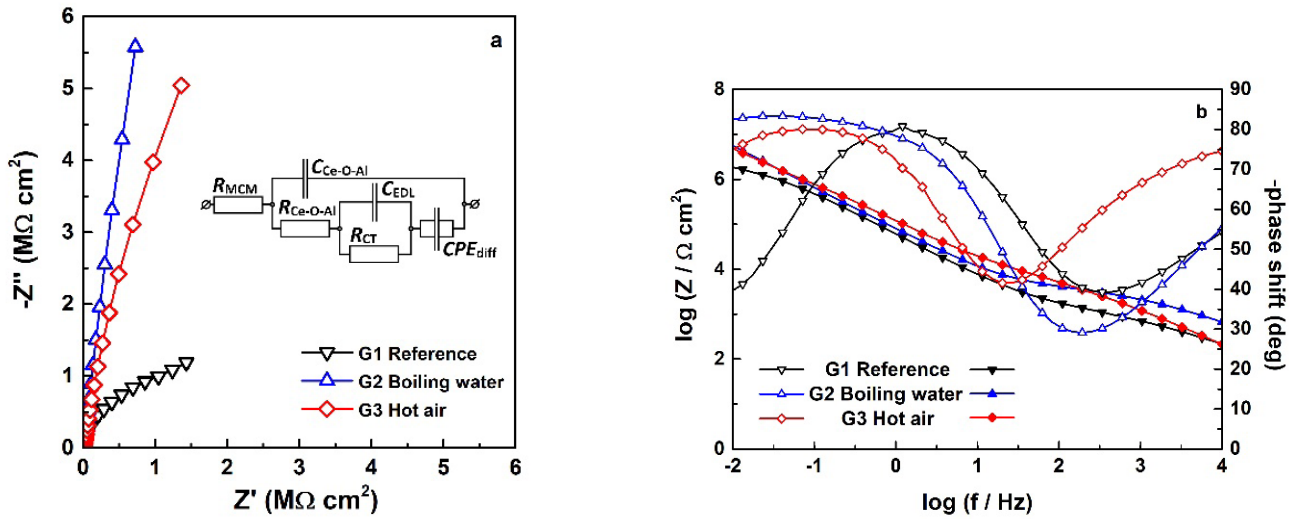

Fig. 2. EIS spectra, plotted in *Nyquist* (a) and in *Bode* (b) coordinates, acquired after 672 hours of exposure to a 5 % NaCl model corrosive medium.

As it can be seen from Table 3, all samples are relatively bright, with values of the parameter L^* above 82. Regarding the parameter a^*, the samples have a negligible greenish hue, probably due to traces of CuO originating from the alloy composition. A unique distinguishable alteration was observed for the parameter b^*, that decreased from above 44 to under 30 after the final thermal treatments. Indeed, the color of the combined layer changes after the respective treating.

The measurements of the average contact angle (θ_{av}) show that all the samples are definitively hydrophilic (Table 3). This property is even further enhanced by treating the samples in boiling distilled water (G_2-BW). This procedure undoubtedly causes a hydration of the coated surface, converting it from hydrophilic to almost super hydrophilic.

Comparative assessment of the corrosion protective properties

This assessment was performed in the course of 672 hours of exposure to a 5 % NaCl model corrosive medium. The acquired EIS spectra are illustrated in Fig. 2.

The *Bode* plots (Fig. 2(a)) reveal that both types of samples (G_2-BW and G_3-HA), that underwent thermal treatment differ from the referent one (G_1-Ref). The observed differences are even more notable in the *Nyquist* diagram (Fig. 2(a)). Unlike the references, these samples demonstrate regular capacitive behavior. This fact shows that the thermal treatments affect the properties of the coatings and thus their performance in the model corrosive medium.

Further, all acquired spectra were submitted to quantitative analysis, through fitting to an appropriate Model Equivalent Circuit (MEC), which is presented in the inset of Fig. 2(a). In the present case, it is composed of $\boldsymbol{R_{MCM}}$ – resistance of the model corrosive medium; $\boldsymbol{C_{Al_2O_3/CeCC}}$ - capacitance of the respective combined layer, due to its insulation properties, $\boldsymbol{R_{Al_2O_3/CeCC}}$ - resistance of the electrolyte, entrapped inside the coating's pores and defects, $\boldsymbol{C_{EDL}}$ - capacitance of the electric double layer, formed underneath the pores of the oxide layer, $\boldsymbol{R_{ct}}$ - charge transfer resistance and $\boldsymbol{CPE_{diff}}$ - a constant phase element, related to the diffusion of corrosive species through the pores once they reach the

Table 4. Data acquired from the electrochemical impedance spectra recorded after 672 hours of exposure of the investigated specimens.

Group	Sample	R_{MCM} [Ω cm^2]	$C_{Al_2O_3/CeCC}$ [nF cm^{-2}]	$R_{Al_2O_3/CeCC}$ [Ω cm^2]	C_{EDL} [μF cm^{-2}]	R_{ct} [MΩ cm^2]	CPE_{diff} [s^n Ω^{-1} cm^{-2}] 10^{-6}	n_{CPE} /
G_1-Ref	S_1	110.2 ± 12.8	119.6 ± 7.0	798.0 ± 45.8	4.3 ± 0.3	1.2 ± 0.1	10.4 ± 0.1	0.47 ± 0.01
	S_2	143.6 ± 16.7	97.3 ± 5.5	1104.0 ± 54.3	4.9 ± 0.5	1.9 ± 0.3	9.4 ± 0.5	0.48 ± 0.01
	S_3	154.1 ± 29.1	97.3 ± 2.7	1220.6 ± 18.7	5.3 ± 0.1	1.3 ± 0.2	8.6 ± 0.5	0.34 ± 0.01
G_2-BW	S_1	287.5 ± 53.3	24.8 ± 1.7	2477.0 ± 378.9	0.2 ± 0.1	23.5 ± 4.5	19.0 ± 9.7	0.71 ± 0.01
	S_2	273.1 ± 36.6	33.2 ± 2.1	3260.0 ± 227.2	0.2 ± 0.1	36.0 ± 9.7	21.6 ± 3.0	0.75 ± 0.01
	S_3	211.3 ± 39.9	27.3 ± 1.9	2280.5 ± 131.3	0.3 ± 0.1	28.7 ± 5.6	31.6 ± 3.5	0.74 ± 0.01
G_3-HA	S_1	56.4 ± 7.7	85.9 ± 2.4	1674.0 ± 123.0	2.5 ± 0.5	(2.9 ± 0.6) 10^{-3}	1.8 ± 0.1	0.79 ± 0.01
	S_2	59.8 ± 9.9	80.8 ± 1.7	1808.0 ± 151.7	2.6 ± 0.1	(8.2 ± 0.4) 10^{-3}	2.2 ± 0.1	0.88 ± 0.01
	S_3	56.2 ± 11.2	83.5 ± 1.1	1633.0 ± 335.2	2.6 ± 0.1	(11.4 ± 0.5) 10^{-3}	2.5 ± 0.1	0.76 ± 0.01

bottom of the oxide layer and its defects. The collected data have been summarized in Table 4.

The highest R_{MCM} values belong to the samples treated in boiling water, most probably due to the hydration processes proceeding along this treatment procedure. Supplemental contribution is also possible by thickening of the dense AAO sublayer under the pores due to additional oxidation. This suggestion is confirmed by the lowest values for the samples, treated in hot air. The latter results in drying of the coating, including removal of any crystal hydrate water. The lowest $C_{Al_2O_3/CeCC}$ values belong to G_2-BW, consequently this layer possesses the highest capacitive reactance, again caused by layer hydration. The same trend is notable for the $R_{Al_2O_3/CeCC}$. The C_{EDL} and R_{ct} reveal the most significant deviations, and their values for G_2-BW differ from those of the rest of the sample sets by entire orders of magnitude, corresponding to the highest capacitive reactance and ohmic resistance, respectively. The CPE_{diff} values of the samples treated in boiling water are higher, revealing easier access of the corrosive species to the metallic surface, probably due to a multitude of defects, formed by the treatment in boiling water. The exponential multiplier (n) of CPE_{diff} for both thermally treated samples approaches unit ($n \rightarrow 1$), meaning that the CPE_{diff} element in both cases (G_2-BW and G_3-HA) resembles a pure capacitor, unlike the referent combined layers.

The potentiodynamic polarization (PDP) curves reveal that after 672 hours of exposure of the samples to the model corrosive medium, the reference samples (G_1-Ref) and those treated in hot air (G_3-HA) indicate clear features of pitting corrosion, whereas those, submitted to boiling water (G_2-BW) reveal no traces of localized corrosion. As evident from Fig. 3, the respective PDP curves of G_2-BW are smooth and almost horizontal, suggesting complete passivation of the sample surface, including the AAO layer defects reparation.

The potentiodynamic curves were subjected to quantitative *Tafel*-slope analysis, in order to acquire precise numerical values for the corrosion potential (E_{corr}), for the pitting nucleation potential (E_{pit}), the strength of pitting corrosion $|E_{corr} - E_{pit}|$ and the polarization resistance (R_p). The obtained data are summarized in Table 5.

Here, it can be inferred that the strength of pitting nucleation $|E_{corr} - E_{pit}|$ in the case of the samples treated

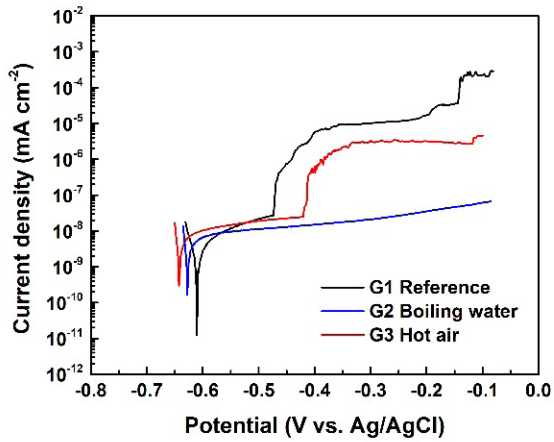

Fig. 3. Potentiodynamic polarization curves acquired after 672 hours of exposure of the samples to the model corrosive medium.

in hot air (G_3-HA) is about twice as large as this of the reference specimens (G_1-Ref), although E_{corr} and E_{pit} possess quite similar values. This discrepancy can be explained assuming a simultaneous shift of E_{corr} and E_{pit} in opposite directions (in other words, more negative E_{corr} values correspond to more positive E_{pit} values). Hence, the treatment in hot air (G_3-HA) results in an increase of the degree of pitting corrosion. Therefore, the treatment in boiling water (G_2-BW) appears to be the preferable approach, since in this case no pitting was detected.

Durability tests

The regular evaluations of the electrochemical parameters have shown lack of notable decrease in their values. Fig. 4 demonstrates excellent overlapping spectra, recorded after 1344 hours of exposure of Sample 3 from the G_2-BW group to the 5 % NaCl solution.

In order to complete the durability tests, all EIS spectra were submitted to quantitative analyses, in accordance to the MEC, illustrated in the inset of Fig. 2(a). The acquired results are summarized in Table 6.

The results in Table 6 confirm the conclusion regarding the subtle variations between the spectra of the combined Al_2O_3/CeCC coating primers sealed by boiling in distilled water, recorded from the beginning (after 24) to the end (after 1344 hours) of exposure to the MCM. Both Fig. 3 and Table 6 show that these samples keep their spectra unchanged during the entire exposure period. The spectra almost completely overlap and the MEC values in Table 6 remain in the same order of magnitude.

The potentiodynamic polarization (PDP) curves, shown in Fig. 5, confirm the assumptions about the corresponding EIS spectra.

The PDP curves, shown in Fig. 5 were submitted to further *Tafel* slope analysis (the data are presented in Table 7), in order to acquire the values of the respective corrosion potential (E_{corr}) and polarization resistance (R_p).

The values of E_{corr} reveal a shift in negative direction, due to the penetration of corrosive species through the defects of the hydrated in boiling water combined layer. Thus, the components of the model corrosive medium reach the metallic surface. The interaction of the MCM species with the cathodic intermetallics underneath the imperfections of the Al_2O_3/CeCC results in shifting of E_{corr} in negative direction. After a certain time (in this case 672 hours of exposure), this shift decelerates

Table 5. Values of the electrochemical variables acquired from the *Tafel*-slope analysis.

Group	Sample	E_{corr} [mV]	E_{pit} [mV]	$\lvert E_{corr} - E_{pit} \rvert$ [mV]	R_p [MΩ cm^2]
G_1-Ref	S_1	-596	-475	121	1.38
	S_2	-575	-443	132	2.05
	S_3	-626	-501	125	1.12
G_2-BW	S_1	-585	----	----	2.55
	S_2	-590	----	----	3.70
	S_3	-627	----	----	1.99
G_3-HA	S_1	-675	-480	195	1.46
	S_2	-642	-420	222	1.28
	S_3	-599	-450	194	1.79

Table 6. Data acquired from the electrochemical impedance spectra obtained after different times of exposure of the Al_2O_3/CeCC coating submitted to treatment in boiling water.

Exposure time	R_{MCM} [Ω cm^2]	$C_{Al_2O_3/CeCC}$ [nF cm^{-2}]	$R_{Al_2O_3/CeCC}$ [Ω cm^2]	C_{EDL} [μF cm^{-2}]	R_{ct} [MΩ cm^2]	CPE_{diff} [s^n Ω^{-1} cm^{-2}] 10^{-6}	n_{CPE} /
24 h	172.0 ± 22.3	41.4 ± 2.4	1125.0 ± 103.0	0.3 ± 0.1	28.84 ± 4.9	17.38 ± 1.5	0.76 ± 0.01
168 h	191.0 ± 24.6	38.5 ± 2.2	1361.5 ± 129.3	0.3 ± 0.1	29.42 ± 5.5	20.29 ± 2.2	0.74 ± 0.01
336 h	210.0 ± 30.5	35.5 ± 2.1	1598.0 ± 155.5	0.3 ± 0.1	29.99 ± 6.0	23.21 ± 2.8	0.75 ± 0.01
504 h	213.0 ± 35.1	30.9 ± 2.1	1685.0 ± 224.2	0.3 ± 0.1	28.87 ± 5.8	28.38 ± 3.4	0.76 ± 0.01
672 h	211.3 ± 39.9	27.3 ± 1.9	2280.5 ± 131.3	0.3 ± 0.1	28.70 ± 5.6	31.60 ± 3.5	0.74 ± 0.01
840 h	205.6 ± 45.0	24.3 ± 1.9	1357.0 ± 214.3	0.3 ± 0.1	29.07 ± 5.7	33.10 ± 3.3	0.75 ± 0.01
1008 h	229.7 ± 41.0	28.2 ± 1.9	1774.0 ± 285.6	0.3 ± 0.1	24.71 ± 4.6	34.08 ± 4.4	0.75 ± 0.01
1176 h	218.0 ± 47.4	28.2 ± 2.1	1447.5 ± 297.3	0.3 ± 0.1	25.50 ± 4.7	35.90 ± 4.0	0.75 ± 0.01
1344 h	216.3 ± 53.1	23.0 ± 2.3	1074.0 ± 288.1	0.3 ± 0.1	25.50 ± 4.9	37.69 ± 3.8	0.74 ± 0.01

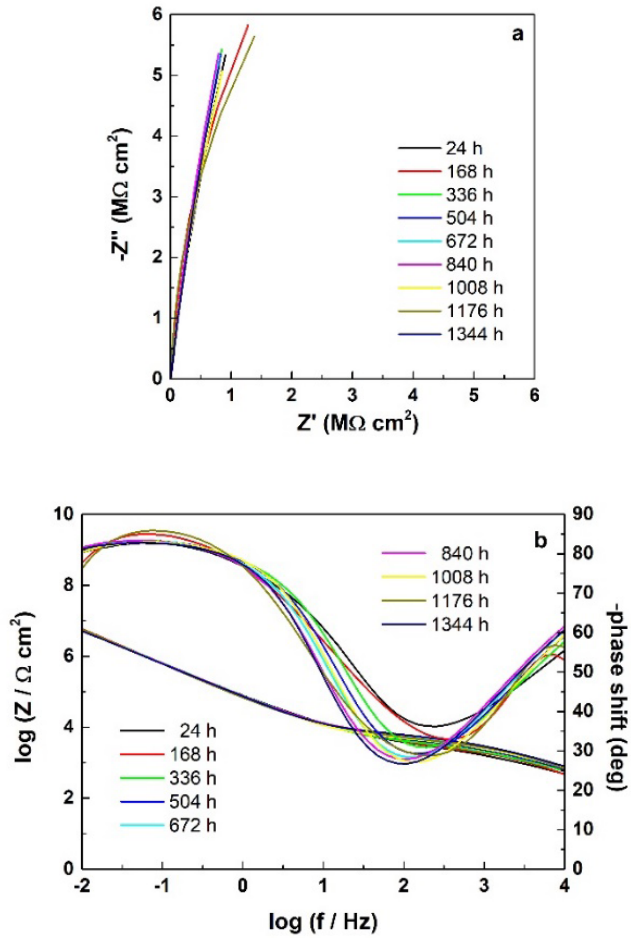

Fig. 4. EIS spectra in *Nyquist* (a) and in *Bode* (b) coordinates recorded for combined Al_2O_3/CeCC coating, treated by boiling for 15 minutes in distilled water.

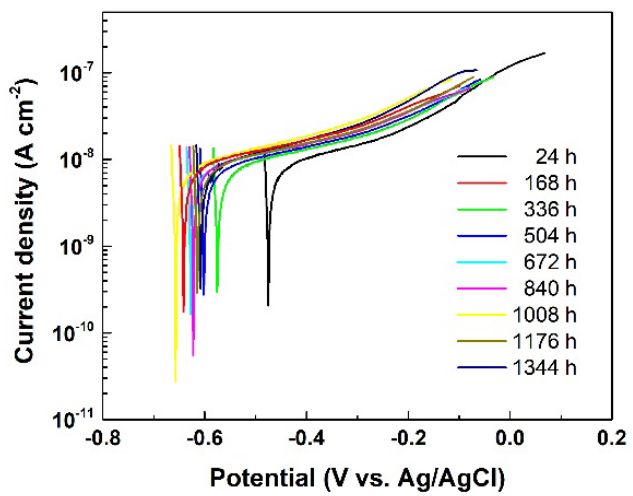

Fig. 5. Potentiodynamic *Tafel*-plots acquired after different times of exposure of the G_2-BW sample to the model corrosive medium.

Table 7. Results of the *Tafel* slope analyses of the potentiodynamic polarization curves, acquired from the G_2-BW sample after extended exposure to a 5 % NaCl solution.

Parameter	Time [hours]								
	24	168	336	504	672	840	1008	1176	1344
$\mathbf{E_{corr}}$ [mV vs. Ag/AgCl/KCl]	-450	-475	-575	-602	-627	-622	-621	-624	-628
$\mathbf{R_p}$ [MΩ cm^2]	0.92	1.43	3.18	1.88	1.99	1.70	2.51	3.09	1.68

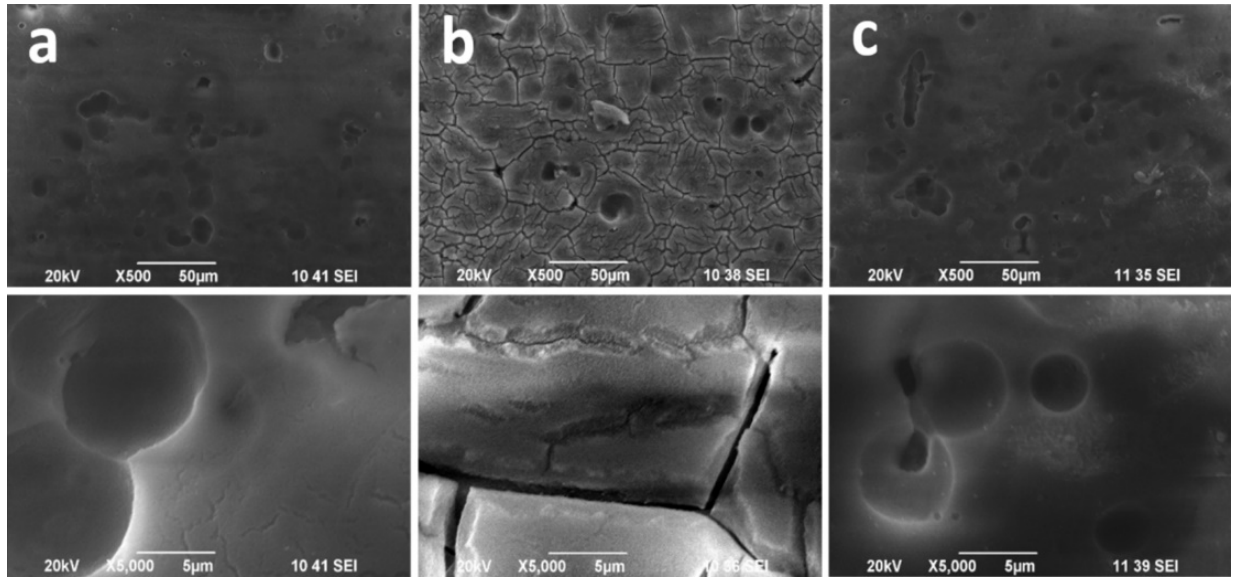

Fig. 6. Secondary electron images of SEM observations performed at low and high magnifications on the following samples: a) G_1-Ref, b) G_2-BW and c) G_3-HA.

due to the covering of the respective anodic areas with corrosion products, thereby suppressing the entire corrosion process.

The fluctuations of R_p are a consequence of the continuous competition between pitting nucleation and re-passivation underneath the ruptures, cracks and other defects of the sealed coating. This assumption is in agreement with the basic concepts regarding the nature of pitting corrosion, described by Frankel [46] and Sklarska-Smialowska [47]. Indeed, the multicomponent composition of the highly-doped AA2024-T3 alloy predetermines the appearance of local corrosion under the defects of the coating [48 - 51]. Hence, although the anodization results in copper depletion from the basic alloy composition [52], the rest, less active alloying elements probably remain on the alloy's surface. This assumption seems reasonable, keeping in mind the multitude of intermetallic phases present in the alloy's composition [48, 53, 54]. The nucleation of local corrosion under the defects of the combined coating is strongly suppressed by the boehmite, formed during the treatment in boiling water, as proposed by Caubert et al. [55]. Besides, supplemental suppression of the localized corrosion appears due to the formation of Keggin type $(Al_{13}O_4(OH)_{24}(H_2O)_{12})^{7+}$, $(AlO_4Al_{12}(OH)_{24}(H2O)_{12})^{7+}$ polyhydroxychlorides during the extended exposure to the 5 % NaCl model corrosive medium, as proposed in previous works [56, 57].

Surface morphology

The surfaces of samples from the three investigated sets were examined by means of Scanning Electron Microscopy. The acquired images are presented in Fig. 6.

The low magnification images (Fig. 6, upper row) show typical pits, formed during the preliminary alloy treatment. Such pits have been observed in previous investigations, as well [45]. The images of the sample, treated in boiling water differ from those of the other samples. The former ones have shown a reticulated morphology, due to the multiple ruptures occurring

Table 8. Surface compositional data, acquired by XPS analysis.

Group	Sample	O [at. %]	N [at. %]	S [at. %]	Al [at. %]	Ce [at. %]	% Ce^{4+}
G_1-Ref	S_1	70.6	1.1	2.0	23.1	0.7	84*
	S_2	62.1	1.4	2.5	29.8	0.9	
G_2-BW	S_1	70.2	-	1.1	27.5	0.2	95*
	S_2	66.7	-	1.2	30.6	0.2	
G_3-HA	S_1	71.4	0.9	-	21.6	0.9	93*
	S_2	65.3	1.1	-	26.1	1.1	

**The respective percentages are represented as a part of the Ce(IV) compounds, relative to the total cerium content.*

during the treatment in boiling water. The strongly hydrated surface probably undergoes swelling when brought in contact with the boiling water. Therefore, after this treatment, the coating is subjected to considerable mechanical stresses due to its subsequent shrinkage.

Compositional analysis

This analysis was performed by XPS on two samples of each type. The acquired quantitative data are presented in Table 8.

The data presented in Table 8 reveal that the predominant components on the surfaces of all samples are oxygen and aluminum. The maximum Al content reaches almost 31 % in the case of the G_2-BW sample. At the same time, the Al:O ratio is nearly 1:2. This is a deviation from the expected ratio for Al_2O_3. These facts reveal that in part the anodized oxide layer still remains uncovered beneath the defects of the Ce-oxide/hydroxide upper layer. The deviation of the oxygen content from the expected is more a result of hydration of the layer due to the use of aqueous solutions and electrolytes than a result of other oxides. Indeed, the cerium amount is quite low and does not contribute sufficiently to a change in the total oxygen content. This inference is further confirmed by the fact that the samples treated in boiling water have a lower Al content, compared to that of oxygen. In other words, the treatment in boiling water leads to an abundance of oxygen in this layer, in the form of both hydroxyl groups and adsorbed water.

The oxidation states of these elements were submitted to further, more detailed analysis. For this purpose, their spectra were subjected to deconvolution, and the results are presented in Fig. 7.

The Al2p spectra show that both samples' surfaces: these of the reference samples (G_1-Ref) and of the ones treated in boiling water (G_2-BW) reveal occurrence of metallic aluminum, indicated by the peaks at 72.9 eV and 72.4 eV, respectively [57]. No traces of elemental Al^0 were detected on the G_3-HA samples. This fact suggests that the exposure to hot air results in the complete oxidation of the formed Al_2O_3/CeCC layer. The peaks, at binding energies in the interval 73.4 - 73.9 eV for all samples correspond to oxidized aluminum Al^{3+} [57 - 60]. The lower energy of these peaks, as well as the ratio of their area to that of the pure Al_2O_3 in the O1s spectrum at around 530.6 eV - 531.7 eV [61, 62] reveal oxygen depletion around the Al^{3+} ions. Limited quantities of boehmite probably occur on the surface of the combined Al_2O_3/CeCC film. Deconvolution of the acquired spectra of samples G_1-Ref and G_3-HA has shown a third peak at 74.7 eV. Its occurrence is related to Al-hydroxides [63]. This peak was not observed in the case of the sample, treated in hot water. The thermal treatment in boiling water probably causes the removal of $Al(OH)_3$, due to its low adhesion to the sample surface.

The comparison of the areas of the Al2p peaks, characteristic for $Al(OH)_3$ to these of the deconvoluted O1s spectrum at 532 - 532.9 eV (Fig. 6, O1s) again reveals excess aluminum, compared to pure $Al(OH)_3$. The peaks in the interval 529.4 - 530.4 eV originate from Ce-O bonds. The other peaks observed in the deconvoluted O1s spectrum in the range 532.8 - 534.3 eV are related to oxygen, in the form of various oxides, such as SiO_2, sulphates, water and others.

The Ce3d spectra, shown in Fig. 8 are rather complex since the peak is at a spin–orbit split into a

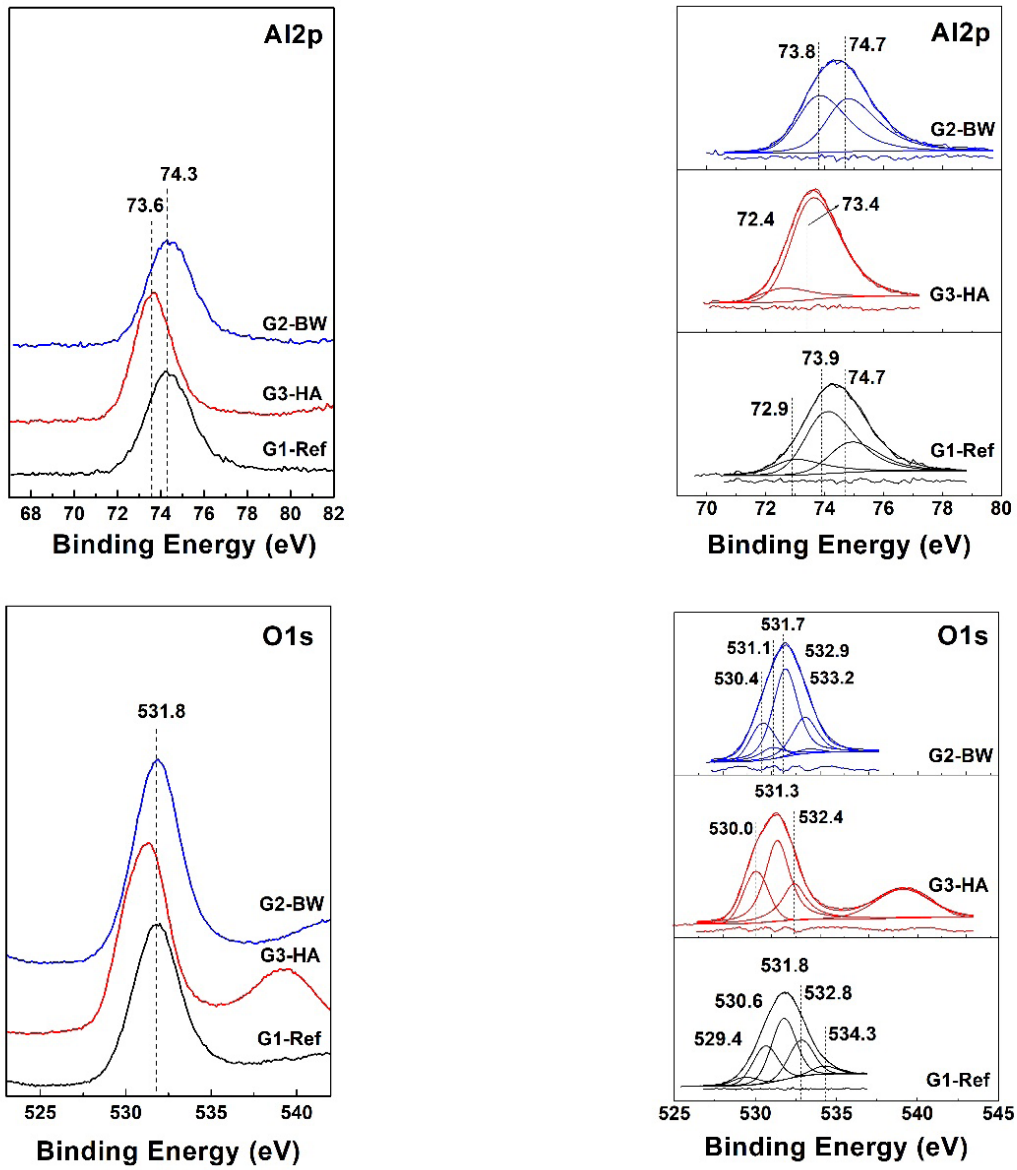

Fig. 7. Integral (a) and deconvoluted (b) XPS spectra of Al2p and O1s.

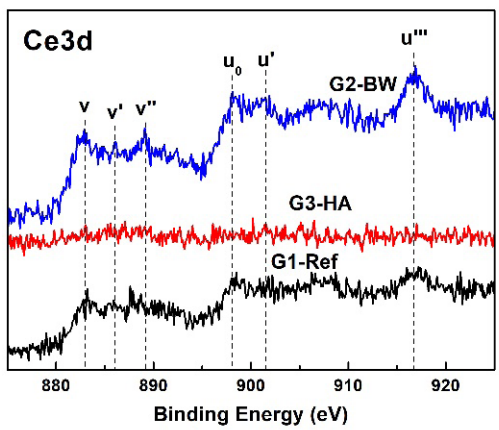

Fig. 8. XPS spectra of ceria acquired from the investigated compounds.

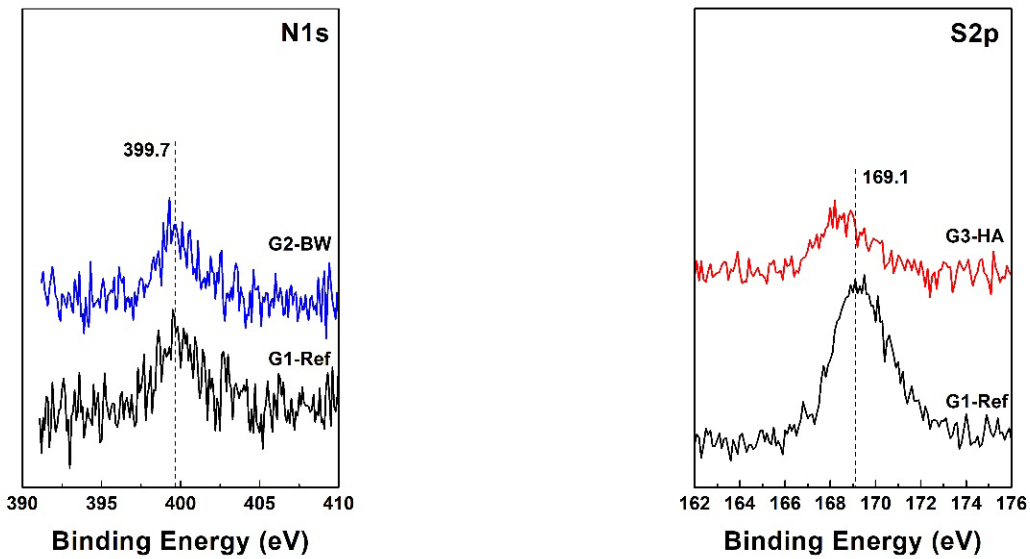

Fig. 9. S2p and N1s spectra acquired from the specimens investigated.

doublet, where each doublet shows extra structures due to final state effects [64, 65]. The principal (*u* and *v*) labels, correspond to a spin-orbital pairs split, while the superscripts denote the final state occupied. Up to ten peaks can be distinguished in the spectra for the sample with high ceria content [65, 66]. They arise from the two oxidation states of cerium present in the films, namely Ce^{3+} and Ce^{4+}.

The doublets labeled as (v^{III} and u^{III}) are typical for CeO_2 and result from a $Ce3d^9O2p^6Ce4f^0$ final state. The v^{III} and u^{III} peaks are the best distinguished characteristic peaks that differentiate Ce^{4+} from Ce^{3+}. When the Ce3d line is detected in a sample with a low Ce content, it has only four peaks because the Ce $4f^0$ final state component is lacking. The area of the u^{III} peak at 916.7 eV is employed to calculate the percentage of Ce^{4+} from the total Ce-content, the results are presented in Table 8. The data reveal that both thermal treatments result in the complete oxidation of the entire Ce amount to Ce(IV) oxides/hydroxides.

The deconvolution of the S2p spectrum, shown in Fig. 9 reveals the presence of three peaks for the reference specimen and four for the one treated in boiling water. The peaks at 167.0 - 167.3 eV are characteristic for the SO_3^{2-} moieties, these at 168.4 - 168.6 eV are typical for $S_2O_3^{2-}$ and those at 169.6 - 170.2 eV reveal the presence of SO_4^{2-} compounds [67, 68]. Obviously, these compounds originate from the reduction of sulphates, which proceeds simultaneously with the oxidation of the Ce(III) compounds to Ce(IV). The additional peak in the spectrum of the reference sample at 170.8 eV originates from the O=C=S compound. The latter is clearly decomposed during the subsequent thermal treatments and does not appear in the cases of G_2-BW and G_3-HA.

The position of the peaks of N1s reveal the presence of nitrogen, in the form of metallic nitrates and/or nitrites [69, 70]. These nitrogen compounds originate from the $Ce(NO_3)_3$, used for the formation of a Al-O-Ce layer, rather than from the HNO_3, used in the preliminary surface treatment of the alloy.

CONCLUSIONS

The present research outlines the results of measurements performed in order to assess the impact of thermal treatment on combined Al_2O_3/CeCC films, their characteristics and performance in a model corrosive medium. The preliminary measurements show that the bright yellow color becomes less intense after thermal treatments. Furthermore, as far as the wettability of the investigated coatings is concerned, immersing them in boiling water converts them from hydrophilic to almost superhydrophilic.

The electrochemical measurements show the significant enhancement of the durability of the combined coatings caused by the applied thermal treatments. Besides, the results highlight the superior effect of treatment in boiling water compared to exposure to hot air. The results from the electrochemical impedance spectroscopy have shown that the thermal treatment leads

to a purely capacitive behavior of the respective samples.

These EIS results have been subjected to further analysis by composing a suitable model equivalent circuit. The analysis has shown that the impedance parameters, acquired for the samples treated in hot water differ from those, characteristic for the other types and reveal their superior performance in the model corrosive medium.

The subsequent potentiodynamic polarization curves have revealed that after 672 hours of exposure to the MCM, the Al_2O_3/CeCC films treated in boiling water do not show any signs of localized corrosion.

Further durability tests performed for up to 1344 hours of exposure to the 5 % NaCl model corrosive medium show lack of any notable changes of the samples' parameters, determined by means of electrochemical measurements.

Although, the SEM images show a multitude of cracks on the samples subjected to treatment in boiling water, it has been determined by additional analytical methods, that these defects are completely re-passivated and/or filled by hydrate layers.

The sample characterizations have been completed by XPS compositional analyses. The results have shown that aluminum is present on the surface of the samples in form of various compounds, and almost all Ce content appears in the form of Ce(IV) oxides/hydroxides. After the subsequent thermal treatments, the Ce(IV) oxides/hydroxides reach almost 100 % of the entire Ce content. It was also established that the reference films contain sulfur and nitrogen inclusions. The sulfur and nitrogen incorporated during the Al_2O_3/CeCC film formation disappear by heating in air or in boiling water, respectively.

The results show, that regardless of the appearance of cracks, the coatings treated in boiling water possess a superior corrosion protective ability, evinced after 672 hours of exposure to a 5 % NaCl model corrosive medium, as well as remarkable durability even after 1344 hours of exposure to the same corrosive medium.

Acknowledgements

The authors express their gratitude to the Bulgarian National Science Fund for the financial support (contract КП-06-Н37/16, 2019). Part of the research was conducted with equipment delivered under the BG-RRP-2.004-0002 BiOrgaMCT project.

REFERENCES

1. M. Bethencourt, F.J. Botana, J.J. Calvino, M. Marcos, M.A. Rodriguez-Chacon, Lanthanide compounds as environmentally-friendly corrosion inhibitors of aluminium alloys: a review, Corros. Sci., 40, 1998, 1803-1819. https://doi.org/10.1016/S0010-938X(98)00077-8.
2. C.E. Castano, W.G. Fahrenholtz, M.J. O'Keefe, Chapter 6 - Ceria-based coatings and pigments, in: S. Scirè, L. Palmisano (Eds.), Cerium Oxide (CeO_2): Synthesis, Properties and Applications, Metal Oxides, Elsevier, 2020, 211-257. https://doi.org/10.1016/B978-0-12-815661-2.00006-2.
3. J.J. Alba-Galvín, L. González-Rovira, F.J. Botana, M. Lekka, F. Andreatta, L. Fedrizzi, M. Bethencourt, Application of Commercial Surface Pretreatments on the Formation of Cerium Conversion Coating (CeCC) over High-Strength Aluminum Alloys 2024-T3 and 7075-T6, Metals, 11, 6, 2021, 930. https://doi.org/10.3390/met11060930.
4. F. Presuel-Moreno, M.A. Jakab, N. Tailleart, M. Goldman, J.R. Scully, Corrosion-resistant metallic coatings, Materials Today, 11, 2008, 14-23. https://doi.org/10.1016/S1369-7021(08)70203-7.
5. R. Andreeva, E. Stoyanova, A. Tsanev, D. Stoychev, On the role of pre-treatment of aluminum substrate on deposition of cerium based conversion layers and their corrosion-protective ability, Int. J. Electrochem. Sci., 13, 2018, 5333-5351. https://doi.org/10.20964/2018.06.71.
6. R. Andreeva, E. Stoyanova, A. Tsanev, D. Stoychev, Influence of the surface pre-treatment of aluminum on the processes of formation of cerium oxides protective films, J. Phys. Conf. Ser., 700, 2016, 012049. https://doi.org/10.1088/1742-6596/700/1/012049.
7. M.A. El-Hashemy, A.E. Hughes, T. Gengenbach, A.M. Glenn, I.S. Cole, Combined influence of Ce(III) and iodide ions for corrosion protection of AA 2024-T3 in acidic to neutral chloride-rich environments: Electrochemical and surface characterization studies, J. Rare Earths, 41, 2023, 309-320. http://DOI10.1016/j.jre.2022.05.014
8. S. Zheng, F. Zhang, Y. Liu, S. Ouyang, Y. W. Ye, H. Chen, Synthesis of Ce, N co–doped carbon dots as green and effective corrosion inhibitor for copper in acid environment, J. Taiwan Institute

Chem. Eng. 141, 2022, Art. No: 104608. https://doi.org/10.1016/j.jtice.2022.104608

9. I. Milosev, B. Kapun, P. Rodic, The Relation Between the Microstructure of Aluminum Alloy 7075-T6 and the Type of Cerium Salt in the Formation of the Cerium Conversion Layer, Journal of the Electrochemical Society, 169, 2022, Art. No: 091501. http://DOI10.1149/1945-7111/ac8d35
10. J. Wang, J. Zhao, M. Tabish, F. Shi, Q. Cheng, L. Peng, Protection of Zn–Mg–Al coated steel corrosion by cerium gluconate in 0.05 M NaCl solution, Journal of Molecular Liquids, 3611, 2022, Art. No: 119595. http:// DOI10.1016/j.molliq.2022.119595
11. T.V. Nguyen, D.L. Tran, T.A. Nguyen, T.T.H. Nguyen, P.H. Dao, V.P. Mac, M.T. Do, T.M. Nguyen, T.M.L. Dang, Ce-loaded silica nanoparticles in the epoxy nanocomposite coating for anticorrosion protection of carbon steel, Anti-Corrosion Methods and Mater. 69, 2022, 514–5234. http://DOI10.1108/ACMM-03-2022-2629
12. R. Lopez-Sesenes, J.G. Gonzalez-Rodriguez, J.G. Vera-Dimas, R. Guardian-Tapia, L. Cisneros-Villalobos, Organic and inorganic compounds as corrosion inhibitors to reduce galvanic effect for the hybrid structure AA2024-CFPR, J. Electrochem. Sci. Eng., 12, 2022, 343–358. http://DOI10.5599/jese.1126
13. M.A.A. Khan, O.M. Irfan, F. Djavanroodi, M. Asad, Development of Sustainable Inhibitors for Corrosion Control, Sustainability (Switzerland), 14, 2022, Art. No: 9502, http://DOI10.3390/su14159502
14. P.J. Denissen, A.M. Homborg, S.J. Garcia, Requirements for corrosion inhibitor release from damaged primers for stable protection: A simulation and experimental approach using cerium loaded carriers, Surf. Coat. Technol., 430, 2022, Art. No: 127966, http://DOI10.1016/j.surfcoat.2021.127966
15. R.K. Harchegani, A.R. Riahi, Effect of Cerium Chloride on the Self-Corrosion and Discharge Activity of Aluminum Anode in Alkaline Aluminum-air Batteries, J. Electrochem. Soc., 169, 2022, Art. No.030542. http://DOI10.1149/1945-7111/ac5c06
16. X.T. Xu, H.W. Xu, Y. Wang, X.Y. Zhang, X.J. Tan, Cerium chloride and L-arginine as effective hybrid corrosion inhibitor for 5052 aluminum alloy in 3.5% NaCl solution, Internat. J. Electrochem. Sci., 17, 2022, Art. No: 221226. http://DOI10.20964/2022.12.24
17. I.A.W. Ma, Sh. Ammar, S.S.A. Kumar, K. Ramesh, S. Ramesh, A concise review on corrosion inhibitors: types, mechanisms and electrochemical evaluation studies, Journal of Coatings Technol. Res., 19, 2022, 241–268. http://DOI10.1007/s11998-021-00547-0
18. Q. Fang, J. Yang, J. Wang, J. Xu, Research progress of cerium-based passivation methods in metal protection, Surf. Technol., 50, 2021, 119–125. http://DOI10.16490/j.cnki.issn.1001-3660.2021.07.011
19. B. Jegdic, B. Bobic, B. Radojkovic, J. Kovacina, D. Marunkic, Synergistic effect of CeCl3 and benzotriazole on corrosion resistance of naturally aged and artificially aged AA2024 aluminium alloy, Transact. Nonferrous Met. Soc. China, 30, 2020, 1478 – 1490. http://DOI10.1016/S1003-6326(20)65312-2
20. J. Panchal, D. Shah, R. Patel, S. Shah, M. Prajapati, M. Shah, Comprehensive Review and Critical Data Analysis on Corrosion and Emphasizing on Green Eco-friendly Corrosion Inhibitors for Oil and Gas Industries, Jour. Bio-Tribo-Corrosion, 7, 2021, Art. No: 107. http://DOI10.1007/s40735-021-00540-5
21. P. Rodic, M. Lekka, Fr. Andreatta, I. Milosev, L. Fedrizzi, The synergistic effect of cerium acetate and sodium sulphate on corrosion inhibition of AA2024-T3 at various temperatures, Electrochim. Acta, 370, 2021, Art. No: 137664, http://DOI10.1016/j.electacta.2020.137664
22. M. Zorainy, D.C. Boffito, M. Gobara, A. Baraka, I. Naeem, H. Tantawy, Synthesis of a novel Ce(iii)/melamine coordination polymer and its application for corrosion protection of AA2024 in NaCl solution, RSC Adv. 11, 2021, 6330-6345. http://DOI10.1039/d0ra08587a
23. L. Selegard, T. Poot, P. Eriksson, J. Palisaitis, P. O. A. Persson, Z. Hu, K. Uvdal, In-situ growth of cerium nanoparticles for chrome-free, corrosion resistant anodic coatings, Surf. Coat. Technol. 410, 2021, Art. No: 126958. http://DOI10.1016/j.surfcoat.2021.126958
24. H. Wei, J. Tang, X. Chen, Y. Tang, X. Zhao, Y. Zuo, Influence of organic and inorganic cerium salts on the protective performance of epoxy coating, Prog. Org. Coat. 166, 2022, Art. No: 106763. http://DOI10.1016/j.porgcoat.2022.106763
25. P. Zhang, Z. Xu, G. Meng, Y. Wang, J. Wang, Y. Shao, F. Wang, Efficiently Improved Corrosion

Resistance of Electrodeposition Ni-Cu Coatings via Site-Blocking Effect of Ce, Adv. Eng. Mater. 24, 10, 2022, Art. No: 2200109. http://DOI10.1002/adem.202200109

26. P. Rajendran, A. Muthuraj, N. E. Rajagounder, Review on CeO2-Based Corrosion Coatings, Transact. Indian Ceram. Soc. 81, 4, 2022, 158-174. http://DOI10.1080/0371750X.2022.2149623
27. J. Bajat, Advances in processing and characterization of conversion coatings, J. Electrochem. Sci.Eng. 12, 4, 2022, 577–578. http://DOI10.5599/jese.1521
28. A.M. Semiletov, A.A. Kudelina, Yu.I. Kuznetsov, New prospects in the application of superhydrophobic coatings and corrosion inhibitors, Internat. J. Corros. Scale Inhib. 11, 3, 2022, 1388–1400. http://DOI10.17675/2305-6894-2022-11-3-28
29. S. Abirami, T. Bharathidasan, S. Sathiyanarayanan, C. Arunchandran, Cerium Stearate Electrodeposited Superhydrophobic Coatings for Active Corrosion Protection of Anodized AA2024-T3, Corrosion, 77, 10, 2021, 1080-1099. http://DOI10.5006/3799
30. S.V. Harb, M.S. Rodrigues, T.A.C. de Souza, A. Trentin, M.C. Uvida, D.J. Pochapski, S.H. Polcinelli, C.V. Santilli, P. Hammer, Smart PMMA cerium oxide anticorrosive coatings: Effect of ceria content on structure and electrochemical properties, Prog. Org. Coat. 161, 2021, Art. No: 106548, http://DOI10.1016/j.porgcoat.2021.106548
31. Ch. Girginov, S. Kozhukharov, M. Milanes, Durability of anodic aluminum oxide (AAO) films formed on technically pure AA1050 alloy against corrosion, Bulg. Chem. Commun., 50-A, 2018, 6-12
32. S. Kozhukharov, Ch. Girginov, Comparative electrochemical and topographical elucidation of Anodic Aluminum Oxide (AAO) layers formed on technically pure aluminum (TPA) and AA2024-T3 aircraft alloy, Bulg. Chem. Commun., 50-A, 2018, 13-21.
33. R.G. Farrakhov, E.V. Parfenov, A.V. Gusarov, D.M. Lazarev, A.R. Fatkullin, Impedance spectroscopy of the process of hard anodizing of aluminum alloys, Surf. Eng. Appl. Electrochem., 52, 2016, 202-211, https://doi.org/10.3103/S1068375516020058.
34. W.J. Stępniowski, W.Z. Misiolek, The influence of electrolyte usage on the growth of nanostructured anodic films on copper in sodium carbonate aqueous solution, J. Electroanal. Chem., 857, 2020, 113491, https://doi.org/10.1016/j.jelechem.2019.113491.
35. K. Engelkemeier, A. Sun, D. Voswinkel, O. Grydin, M. Schaper, W. Bremser, Zinc Anodizing: Structural Diversity of Anodic Zinc Oxide Controlled by the Type of Electrolyte, Chem. ElectroChem., 8, 2021, 2155-2168, https://doi.org/10.1002/celc.202100216.
36. S.R. Kunst, A.C.V. Bianchin, L.T. Mueller, J.A. Santana, T.M. Volkmer, F.D.P. Morisso, C.L.P. Carone, J.Z. Ferreira, I.L. Mueller, C.T. Oliveira, Model of anodized layers formation in Zn–Al (Zamak) aiming to corrosion resistance, J. Mater. Res. Technol., 12, 2021, 831-847, https://doi.org/10.1016/j.jmrt.2021.03.027.
37. D.I. Petukhov, A.A. Eliseev, I.V. Kolesnik, K.S. Napolskii, A.V. Lukashin, A.V. Garshev, Y.D. Tretyakov, D. Chernyshov, W. Bras, S-F. Chen, C-P Liu, Mechanically stable flat anodic titania membranes for gas transport applications, Journal of Porous Materials, 19, 2012, 71-77, https://doi.org/10.1007/s10934-010-9449-2.
38. I. Sadykov, S.E. Kushnir, N.A. Sapoletova, V.K. Ivanov, K.S. Napolskii, Anodic titania photonic crystals with high reflectance within photonic band gap via pore shape engineering, Scripta Materialia, 178, 2020, 13-17, https://doi.org/10.1016/j.scriptamat.2019.10.044.
39. 39. J.W. Diggle, T.C. Downie, C.W. Goulding, Anodic oxide films on aluminum, Chem. Rev., 69, 1969, 365-405, https://doi.org/10.1021/cr60259a005.
40. C.J. Dell'Oca, D.L. Pulfrey, L. Young, Anodic Oxide Films, Physics of Thin Films 6, 1971, 1–79, https://doi.org/10.1016/B978-0-12-533006-0.50008-6
41. S. Kozhukharov, Ch. Girginov, Enhancement of the cerium oxide primer layers deposited on AA2024-T3 aircraft alloy by preliminary anodization, J. Electrochem. Sci. Eng., 8, 2018, 113-127, https://dx.doi.org/10.5599/jese.478.
42. M. Fedel, J. Franch, S. Rossi, Effect of thickness and sealing treatments on the corrosion protection properties of anodic oxide coatings on AA5005, Surf. Coat. Technol., 408, 2021, 126761, https://doi.org/10.1016/j.surfcoat.2020.126761.
43. S. Ofoegbu, F.A.O. Fernandes, A.B. Pereira, The Sealing Step in Aluminum Anodizing: A Focus on Sustainable Strategies for Enhancing Both Energy Efficiency and Corrosion Resistance, Coatings, 10, 2020, 226, https://doi.org/10.3390/

coatings10030226.

44. S. Kozhukharov, A. Dishliev, Ch. Girginov, Reproducibility of the surface characteristics of anodized aa2024-t3 aircraft alloy with deposited Ce-conversion coating, J. Chem. Technol. Metall. 57, 2022, 353-360
45. E. Matter, S. Kozhukharov, M. Machkova, V. Kozhukharov, Reproducibility of the corrosion parameters for AA2024-T3 aluminium alloy in chloride solution after different preliminary treatment procedures, J. Chem. Technol. Metall., 50, 2015, 52-64.
46. G.S. Frankel, Pitting Corrosion of Metals: A Review of the Critical Factors, J. Electrochem. Soc., 145, 1998, 2186-2198, https://doi.org/10.1149/1.1838615.
47. Z. Szklarska-Smialowska, Pitting corrosion of aluminum, Corros. Sci. 41, 1999, 1743-1767, https://doi.org/10.1016/S0010-938X(99)00012-8
48. J.G. Brunner, N. Birbilis, K.D. Ralston, S. Virtanen, Impact of ultrafine-grained microstructure on the corrosion of aluminium alloy AA2024, Corros. Sci., 57, 2012, 209-214, https://doi.org/10.1016/j.corsci.2011.12.016.
49. A. Rodríguez-Veiga, B. Bellon, I. Papadimitriou, G. Esteban-Manzanares, I. Sabirov, J. LLorca, A multidisciplinary approach to study precipitation kinetics and hardening in an Al-4Cu (wt. %) alloy, J. Alloys Compd., 757, 2018, 504-519, https://doi.org/10.1016/j.jallcom.2018.04.284.
50. M. Fedel, J. Franch, St. Rossi, Effect of thickness and sealing treatments on the corrosion protection properties of anodic oxide coatings on AA5005, Surf. Coat. Technol.408, 2021, Art. No: 126761, http://DOI10.1016/j.surfcoat.2020.126761.
51. O.M. Prada Ramirez, F.M. Queiroz, M.A. Tunes, R.A. Antunes, C.L. Rodrigues, A. Lanzutti, St. Pogatscher, M. Olivier, H. G. De Melo, Tartaric-sulphuric acid anodized clad AA2024-T3 post-treated in Ce-containing solutions at different temperatures: Corrosion behaviour and Ce ions distribution, Appl. Surf. Sci. 534, 2020, Art. No: 147634, http://DOI10.1016/j.apsusc.2020.147634
52. S. Kozhukharov, Ch. Girginov, I. Avramova, M. Machkova, Anodic galvanostatic polarization of AA2024-T3 aircraft alloy in conventional mineral acids, Mater. Chem. Phys., 180, 2016, 301-313, https://doi.org/10.1016/j.matchemphys.2016.06.011.
53. P. Camperstini, E.P.M. van Westing, H.W. van Rooijen, J.H. De Wit, Relation between microstructural aspects of AA2024 and its corrosion behaviour investigated using AFM scanning potential technique, Corros. Sci., 42, 2000, 1853-1861, https://doi.org/10.1016/S0010-938X(00)00002-0.
54. A.E. Hughes, C. MacRae, N. Wilson, A. Torpy, H.T. Muster, A.M. Glenn, Sheet AA2024-T3: a new investigation of microstructure and composition, Surf. Int. Anal., 42, 2010, 334-338, https://doi.org/10.1002/sia.3163.
55. F. Caubert, Pierre-Louis Taberna, L. Arurault, B. Fori, Electrophoretic deposition of boehmite particles to improve the anti-corrosion behavior of anodized aluminum alloy 2024-T3, Bulg. Chem. Commun., 52-E, 2020, 21-27.
56. S. Kozhukharov, V. Kozhukharov, M. Wittmar, M. Schem, M. Aslan, H. Caparrotti, M. Veith, Protective abilities of nanocomposite coatings containing Al_2O_3 nano-particles loaded by $CeCl_3$, Prog. Org. Coat., 71, 2011, 198-205, https://doi.org/10.1016/j.porgcoat.2011.02.013.
57. A.A. Salve, S. Kozhukharov, J.E. Pernas, E. Matter, M. Machkova, A comparative research on hybrid nano-composite protective primary coatings for AA2024 aircraft alloy, J. Univ. Chem. Technol. Met., 47, 2012, 319-326
58. S. Oswald, F. Thoss, M. Zier, M. Hoffmann, T. Jaumann, M. Herklotz, K. Nikolowski, F. Scheiba, M. Kohl, L. Giebeler, D. Mikhailova, H. Ehrenberg, Binding Energy Referencing for XPS in Alkali MetalBased Battery Materials Research (II): Application to Complex Composite Electrodes, Batteries, 4, 2018, 36, https://doi.org/10.3390/batteries4030036.
59. J. Ryl, M. Brodowski, M. Kowalski, W. Lipińska, P. Niedziałkowski, J. Wysocka, Corrosion Inhibition Mechanism and Efficiency Differentiation of Dihydroxybenzene Isomers Towards Aluminum Alloy 5754 in Alkaline Media, Materials, 12, 2019, 3067, https://doi.org/10.3390/ma12193067.
60. A. Kumar, P.C. Srivastava, X-ray photoelectron spectroscopy (XPS) study of Heusler alloy (Co_2FeAl) interfaced with semiconductor (n-Si) structure, Materials Science-Poland, 37, 2019, 116-121, https://doi.org/10.2478/msp-2019-0001.

61. H. Yu, Y. Gao, X. Liang, Slightly Fluorination of Al_2O_3 ALD Coating on $Li_{1.2}Mn_{0.54}Co_{0.13}Ni_{0.13}O_2$ Electrodes: Interface Reaction to Create Stable Solid Permeable Interphase Layer, J. Electrochem. Soc., 166, 2019, A2021-A2027, https://dx.doi.org/10.1149/2.0951910jes.
62. A.H. Alshehri, K. Mistry, V.H. Nguyen, K.H. Ibrahim, D. Muñoz-Rojas, M. Yavuz, K.P. Musselman, Quantum-Tunneling Metal-Insulator-Metal Diodes Made by Rapid Atmospheric Pressure Chemical Vapor Deposition, Advanced Functional Materials, 29, 2018, 1805533, https://doi.org/10.1002/adfm.201805533.
63. T. Tago, N. Katoka, H. Tanaka, K. Kinoshita, S. Kishida, XPS study from a clean surface of Al_2O_3 single crystals, Procedia Engineering, 216, 2017, 175-181, https://doi.org/10.1016/j.proeng.2018.02.081.
64. P. Huestis, C.I. Pearce, X. Zhang, A.T. N'Diaye, K.M. Rosso, J.A. LaVerne, Radiolytic stability of gibbsite and boehmite with adsorbed water, Journal of Nuclear Materials, 501, 2018, 224-233, https://doi.org/10.1016/j.jnucmat.2018.01.043.
65. E. Paparazzo, On the curve-fitting of XPS Ce(3d) spectra of cerium oxides, Materials Research Bulletin, 46, 2011, 323-326, https://doi.org/10.1016/j.materresbull.2010.11.009.
66. E. Paparazzo, Use and mis-use of XPS Ce3d spectra of Ce_2O_3 and CeO_2, J. Phys.: Condens. Matter, 30, 2018, 1-83, https://doi.org/10.1088/1361-648X/aad248.
67. O. Costa-Nunes, R.M. Ferrizz, R.J. Gorte, J.M. Vohs, Structure and thermal stability of ceria films supported on YSZ(100) and α-Al_2O_3 (0001), Surface Science, 592, 2005, 8-17, https://doi.org/10.1016/j.susc.2005.06.029.
68. A. Pardo, S. Feliú Jr., M.C. Merino, R. Arrabal, E. Matykina, The effect of cerium and lanthanum surface treatments on early stages of oxidation of A361 aluminium alloy at high temperature, Appl. Surf. Sci., 254, 2007, 586-595, https://doi.org/10.1016/j.apsusc.2007.06.036.
69. M. Fantauzzi, B. Elsener, D. Atzei, A. Rigoldi, A. Rossi, Exploiting XPS for the identification of sulfides and polysulfides, RSC Adv., 5, 2015, 75953-75963, https://doi.org/10.1039/C5RA14915K.
70. X. Wang, Z. Sun, Y. Zhao, J. Li, Y. Zhang, Z. Zhang, $Na_4Mn_9O_{18}$ nanowires wrapped by reduced graphene oxide as efficient sulfur host material for lithium/sulfur batteries, J. Solid State Electrochem., 24, 2020, 111-119, https://doi.org/10.1007/s10008-019-04478-0.
71. J. Baltrusaitis, P.M. Jayaweera, V.H. Grassian, XPS study of nitrogen dioxide adsorption on metal oxide particle surfaces under different environmental conditions, Phys. Chem. Chem. Phys., 11, 2009, 8295-8305, https://doi.org/10.1039/B907584D.
72. X. Fan, Z. Wu, H. Li, B. Geng, C. Li, P. Yan, Morphology and thermal stability of Ti-doped copper nitride films, J. Phys. D: Appl. Phys., 40, 2007, 3430-3435, https://doi.org/10.1088/0022-3727/40/11/025.